COMMUNICATION

Check for updates

Tetra-benzimidazoles flanking divinyl-phenothiazine: AIEgens as aza-Michael acceptors in concentration-tuned responses to biogenic amine vapors†

Sameer Singh,[a] Kalyaneswar Mandal [iD] [b] and Manab Chakravarty [iD] *[a]

Tetra-benzimidazole rotors flanking a divinyl-phenothiazine stator are realized as red AIEgens and newly identified as efficient aza-Michael acceptors for the identification of biogenic amine vapors. Weakly red-emissive solids display a blue-shifted turn-on emission by rapid aza-Michael addition and simultaneous reverse Knoevenagel reactions. Concentration variation imposes better crystallinity and facilitates radiative decay, offering distinct emissions.

Benzimidazole (BIZ) is a stable functionalized heterocycle with two naturally different nitrogen centers, displaying a myriad of chemical and biological landscapes.[1–4] This building block is renowned as a biologically/therapeutically active substrate.[1] In addition, its optical chemical sensor-based applications are also noteworthy due to the intriguing photophysical features, such as PET (photo-induced electron transfer), ICT (intramolecular charge transfer), and ESIPT (excited state intramolecular proton transfer), associated with BIZ.[5–8] Promising molecular sensors developed on benzimidazole are limited to solution states; therefore, the difficulty in making suitable devices is significant.[7,8] Since the discovery of aggregation-induced emission active fluorogens (AIEgens) in 2001,[9,10] AIEgens have emerged as a new interdisciplinary area, offering a wide range of real-world applications.[11,12]

Numerous heterocycles have been incorporated to construct functionalized AIEgens for optical materials developments.[13,14] However, AIEgens developed from BIZ units, such as **A** and **B** (see Fig. 1), are sporadic.[15,16] Only a few AIEgens are recognized to detect anions and other crucial analytes *via* aggregation–disaggregation mechanisms.[15–17] The AIE event mainly originates from the restricted intramolecular motion (RIM) of the rotors.[11] A literature search revealed an olefin stator, **C**, with four BIZ rotors as a yellow chromophoric dye, which was invented 43 years prior to the

discovery of AIEgens.[17] The molecular structure of **C** is similar to the well-established tetraphenylethylene (TPE) architecture, where BIZ is replaced with a phenyl ring. Such a TPE core is widely applied to create various AIE platforms.[9,11]

Herein, we describe an easily accessible new class of alkene stators symmetrically anchored with a phenothiazine core and holding the BIZ units as rotors. While four BIZ rotors make these molecules nonradiative in solution, the aggregated state make them emissive due to the restricted motion of the rotors. Thus, bis (2-benzimidazolyl)methane (**BIZM**) would be an excellent scaffold for building AIE-active functional materials. Unlike TPE, this new design adopts two tri-substituted olefin stators, where each olefin holds two BIZ and a common phenothiazine (PTZ) rotors (Fig. 1).

Although vinyl dicyano/ester/cyanoester-based fluorescent probes are well explored as aza-Michael acceptors (MA),[18] such bis-dibenzimidazole vinyl systems as MAs are unfamiliar as fluorescent probes. With our recent interest in developing concentration-based biogenic amine (**BA**) sensors,[19] the **BIZM** is installed on a divinyl-phenothiazine core to achieve a new class of red-emissive AIEgens as an MA-based platform, which could be vital to detect crucial BA vapors, such as putrescine

[a] *Department of Chemistry, Birla Institute of Technology and Sciences, Pilani-Hyderabad Campus, Jawahar Nagar, Shamirpet, Hyderabad – 500078, India. E-mail: manab@hyderabad.bits-pilani.ac.in*

[b] *Tata Institute of Fundamental Research Hyderabad, 36/p Gopanpally, Hyderabad, Telangana – 500046, India. E-mail: kmandal@tifrh.res.in*

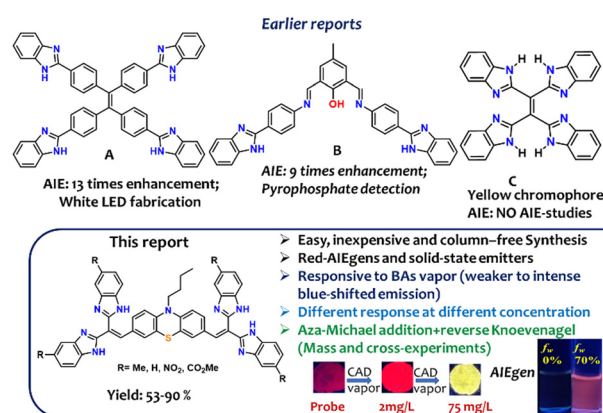† Electronic supplementary information (ESI) available. See DOI: https://doi.org/10.1039/d4cc05725b

Fig. 1 Top: A few relevant benzimidazoles-linked molecules (A)–(C) established as AIEgens and their utility. Bottom: Key points of this report. CAD: cadaverine.

(PUT) and cadaverine (CAD) at different concentrations. These BAs play a key role in indicating the freshness of food and are mainly responsible for food spoilage.[20] These BAs indirectly control the amount of toxic histamine production, which is responsible for scombroid food poisoning.[21] Available standard analytical techniques are inappropriate for onsite applications. Therefore, fluorimetric detection is an emerging requirement to provide a sensitive, simple, handy, and inexpensive detection strategy.[22]

Although the synthetic strategy is well established,[23] we encountered difficulties in achieving **BIZM**. The reported procedures used 1,2-diaminobenzene and malonic acid in the presence of various acid catalysts at 120–150 °C (Fig. S1, ESI†), but none of the results were promising. We could identify many side products from this reaction (as analyzed using mass spectrometry; Fig S2, ESI†). However, replacing malonic acid with malonamide showed improved results, with almost quantitative yields by using triflic acid or PTSA as a selective acid catalyst in 1,4-dioxane under reflux (Fig. S2(i), ESI† and Fig. 2a). As a result, the precursor **BIZM** with electron-donating/withdrawing features is ready without any further purification. Next, the active methylene group of **BIZM**, holding electronically diverse groups was successfully employed in the Knoevenagel reaction to afford tetra(benzimidazole)-linked vinylic PTZ molecules (Fig. 2b) in >90% purity.

The photophysical studies were performed for these tri-substituted functionalized alkenes, which were expected to be emissive aza-MAs. The (solid) molecules absorb at a λ_{max} in the range 465–553 nm (Table S2, ESI†) and emit weakly at λ_{max} of 612–671 nm (red). Although the **PBNO** absorbs at λ_{max} 553, it has no emission, possibly due to spin–orbit coupling of the NO_2 functionality.[24] There was a red-shifted emission in high-polar solvent, indicating the presence of an ICT state, but the solvatochromic features were not valuable with such weakly emissive molecules (Fig. S5, ESI†). Notably, the intramolecular H-bonding for these molecules can strongly govern the dynamics of the electronic states. Specifically, the intramolecular H-bond creates new electronic coupling pathways through donor-H-acceptor complex formation. The intramolecular H-bonds enable rapid internal conversion in a wide range of solvents, resulting in fluorescence quenching.[25] However, the electron-withdrawing effect of ester and chloro groups enabled **PBES** and **PBCl** to display a better red-shifted solvatochromism in both ground and excited states compared to **PBH** and **PBMe**. This confirms a prominent ICT formation between the electron-rich PTZ core and the electron-withdrawing BIZ part. For further conformation, the molecular geometry of **PBES** was optimized using density functional theory (DFT) in dimethylsulfoxide (see computational details in ESI†). The DFT-optimized structure exhibitedd a conformationally twisted geometry of **PBES**, where vinylenic bis(BIZ) units on both sides of the PTZ core slightly deviate from each other in the selective bond lengths and torsion angles (Fig. S6a, ESI†). The highest occupied molecular orbital (HOMO) was confined over the PTZ core, and the BIZ units mainly constructed the lowest unoccupied molecular orbital (LUMO) (Fig. S6b and c, ESI†). Moreover, such a conformationally twisted geometry would facilitate emission in the aggregated state.

The AIE studies were conducted in a binary mixture of THF (good) and water (bad) solvents. The gradual increase of water fraction (f_w in v/v) in 10 μM THF solution of the probe exhibited enhancement in red emission at f_w = 70–80% as follows: **PBH**, 10 times (Fig. S9a, ESI†); **PBES**, 6 times (Fig. S9b, ESI†); **PBMe**, 7 times (Fig. S9c, ESI†); and **PBCl**, 7 times (Fig. 3). The bathochromic shifts in absorption (Fig. S7, ESI†) and emission (Fig. 3a and c) suggest the possible formation of a J-aggregate, increasing the excitonic conjugations.[26] Furthermore, a prominent, visually detectable rise in emission intensity (~7 times) specifies the AIE features of these probes. Dynamic light scattering studies demonstrated an average particle size of ~140–240 nm, proving the nanoaggregate formation (Fig. S10, ESI†). The viscochromic studies (Fig. S11, ESI†) with **PBES** (a representative example) also displayed emission intensity enhancement, indicating the cause of the AIE feature as RIM in the aggregate state.

Next, we concentrated on the solid-state emission features of these molecules, because BA vapor detection needs a solid emissive platform as a desirable strategy for handy, real-life applications.[27] All were weakly red emissive: **PBH**: λ_{max} = 612 nm; absolute quantum yield φ_f (%) = 0.42; **PBES**: λ_{max} = 671 nm; φ_f (%) = 0.09; **PBMe**: λ_{max} = 642 nm; φ_f (%) = 0.46; and **PBCl** λ_{max} = 659 nm; φ_f (%) = 0.17. Although the φ_f (%) is poor, the red emission was visually detectable and thus utilized to sense the BA vapor. However, such α,β-unsaturated probes can be recognized as newly suitable aza-Michael acceptors. Later, the thin film was easily prepared by drop-casting 10^{-3} M acetonitrile solution on a glass coverslip and evaporated to dryness at 25 °C. In a closed jar,
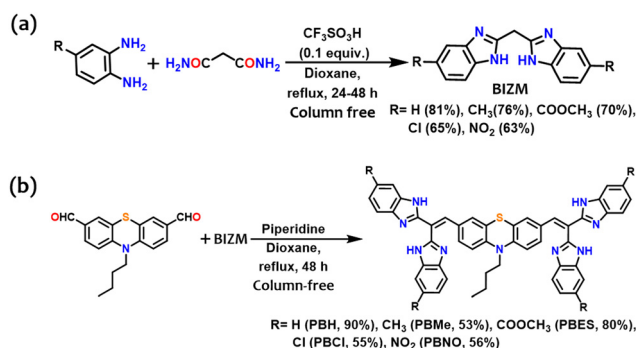

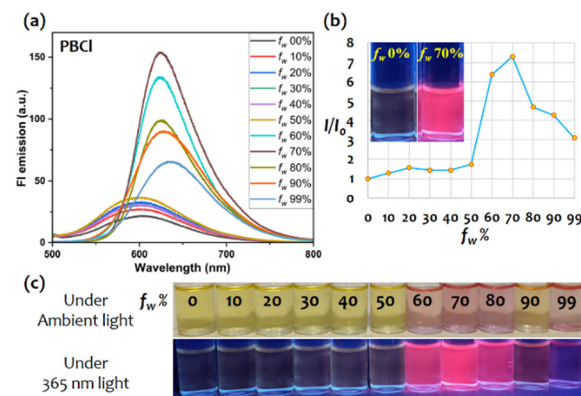**Fig. 2** (a) Modified synthetic strategy for **BIZM**. (b) Synthesis of the emissive probes.

Fig. 3 (a) The change in emission (of **PBCl**) upon increasing water fraction. (b) I/I_0 vs. f_w (%) plot; (inset) the intensity change. (c) The change in emission and absorption color (red) visible to the naked eye.
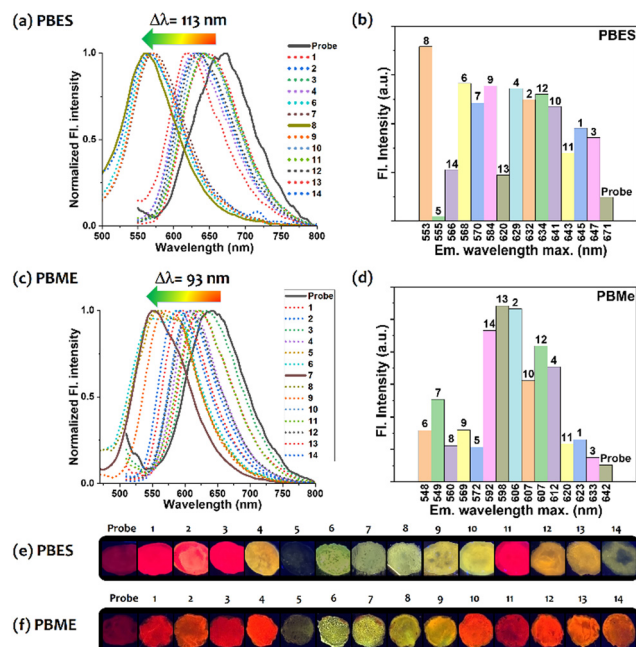
Fig. 4 Exposure to various amine vapors on thin film (See Fig. S13 d, ESI†) and the emission shifts. (a) **PBES** and (c) **PBMe** platform; and (b) and (d) the respective bar-graph for fluorescence intensity *vs.* wavelength maxima. The color change for (e) **PBES** and (f) **PBMe**. Amines used are, 1: NH₃; 2: *N*-butylamine; 3: DIPEA; 4: 2-phenylethylamine; 5: 1,2-ethylenediamine (EDA); 6: DAP; 7: PUT; 8: CAD; 9: 1,6-hexanediamine; 10: spermidine; 11: spermine; 12: 3-aminopropanol; 13: 4-aminobutanol; 14: *N,N*-dimethylaminopropylamine.

the red-emissive film was exposed to various amine vapors (excess; see Fig. 4 for the list) for 4 h to visualize the maximum possible change.

Highly reactive **PBES** exhibited poor selectivity and thus responded against most diamines, including BA vapors (except spermine) and analogous amino alcohols (Fig. 4e). However, **PBMe** (Fig. 4f) was relatively more selective to only volatile diamines, including DAP, PUT and CAD. The response of **PBCl** was similar to that of **PBES**, while the response of **PBH** was comparable to that of **PBMe** (Fig. S12, ESI†). The red emission was either quenched or blue-shifted (90–115 nm; displaying yellow or yellowish-green emission). The emission shift for **PBES/PBCl** was more than for **PBMe/PBH**, as expected. The emission shift was higher and more prominent for **PBES** (113 nm) than for **PBMe** (93 nm). Other common monoamines, such as NH₃, *n*-tylamine, di-isopropylethylamine (DIPEA), and spermine (BA), subtly impacted the emission profiles. Such a difference can be deciphered by considering several parameters, such as steric hindrance, nucleophilicity, vapor pressure, and the affinity of the dye that can tune the response difference towards various amine vapors.[28] However, higher responses with diamine compared to monoamine could be due to significant and influential interactions of the two –NH₂ groups with a benzimidazole-enriched surface and gradually proceeding to the consecutive chemical reactions. Although the monoamine could activate the probe, this may not be enough to change its emission behavior.

Apart from the emission shift, we also noticed a significant increase in the φ_f for the diamine analogs EDA, DAP, PUT, CAD, and DAH (Table S3, ESI†). Thus, this probe is selectively responsive to crucial diamines, such as PUT and CAD, which

primarily originate during food spoilage and are associated with industrial freshness indicators.[29] Next, the concentration of CAD vapor (as a representative BA) was gradually increased and exposed to **PBES** film for 2 h in a sealed chamber. Initially, the red emission intensity (% φ_f = 0.09 to 2.13) was improved to 4 mg L⁻¹ (Fig. 5). In a similar manner, PUT was gradually exposed on PBMe film. The change was slightly different, with red → orange → yellow conversion, exhibiting an admirable %φ_f enhancement up to 5.92, from a value of 0.3. The hypsochromic shift and φ_f improvement with a gradual increment of the BA concentration are noteworthy (Fig. S13–S16, ESI†).

A concentration-based visually detectable emission shift with φ_f heightening would be helpful for onsite applications. A possible reason for this φ_f surge is the development of a supramolecular assembly between the diamine, dye, and intermediates, which enables RIM and prefers relaxation through the radiative decay channel (gradual increase in excited state lifetime and radiative rate constant), as supported by lifetime studies (Fig. S17 and Table S4a, b, ESI†). Thereafter, the observed blue-shifted emission from red to yellow specifies the reduction of π-delocalization, a result of aza-Michael addition (see below). Notably, the response of the probes with these amines in solution state was not impressive (Fig. S18, ESI†). Additionally, the powder X-ray diffraction profiles for weak red to intense red and yellow solids indicate a gradual enhancement in crystallinity (Fig. S22, ESI†), suggesting a possible crystallization-induced emission effect, which was reported earlier for imine-based emitters.[30]

Thus, the affinity of the analyte on the benzimidazole-enriched emissive platform and subsequent aza-Michael and reverse Knoevenagel reaction promote imine formation, leading to a change in emission intensity and wavelength. The **PBES** film exposed to PUT vapor was analyzed to determine the fate of the reaction as an illustrative example. The relatively more intense red-emissive **PBES-R** and yellow-emissive **PBES-Y** were dissolved in DMSO to run through HPLC and injected in LC-MS. The HPLC (Fig. 6i) and LC-MS (Fig. 6ii) profiles designate the difference in the product formation, which was analyzed using LC-MS, showing the red-emissive **PBES-R** as a mixture of (a) **BIZM**, (b) **PBES** (trace), (c) PTZ-monoaldehyde, and (d) PTZ-bisaldehyde (Fig. 6iii). The yellow-emissive **PBES-Y** results from only a mixture of PTZ-bisaldehyde and **BIZM**. The identified aldehyde(s) (d) were attributed to the acid-hydrolyzed product
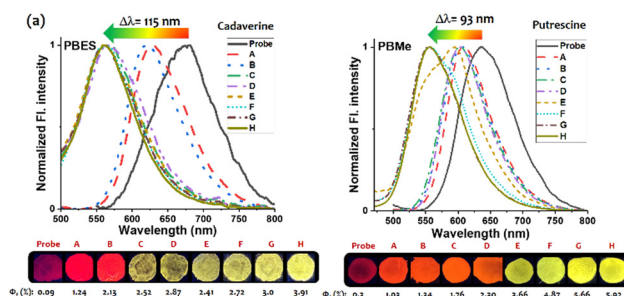

Fig. 5 Gradual increase of CAD concentration for (a) **PBES** and (b) PUT for **PBMe**. Concentrations: A, 2 mg L⁻¹; B, 4 mg L⁻¹; C, 15 mg L⁻¹; D, 25 mg L⁻¹; E, 50 mg L⁻¹; F, 75 mg L⁻¹; G, 100 mg L⁻¹; H, 125 mg L⁻¹. The film is cropped for better presentation.
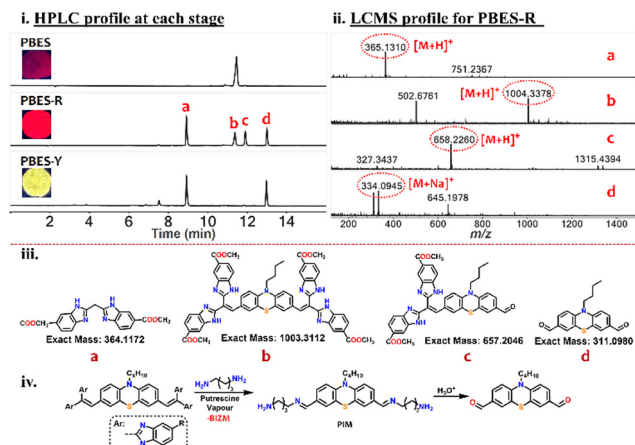
Fig. 6 (i) HPLC profiles at each emissive stage (**PBES**, **PBES-R**, and **PBES-Y**). (ii) LC-MS profile for **PBES-R** (containing all the components, as present in **PBES** and **PBES-Y**). (iii) Structure of product found during the LC-MS monitoring of **PBES-R**. (iv) Reaction scheme of PIM formation in the presence of putrescine vapors and its acid hydrolysis.

of diamine PIM (Fig. 6iv), which is susceptible to hydrolyzing under an acidic environment in the LC column.

Quick aza-Michael addition of BAs to the α,β-unsaturated part of this dye forms a tetrahedral intermediate, reducing the π-conjugation and interpreting the blue-shifted emission. Subsequently, a fast reverse Knoevenagel reaction occurs, liberating **BIZM** (which was formed from a stable carbanion) and producing the corresponding **PIM** (Fig. 7), which undergoes hydrolysis to produce the bisaldehyde, detected in the LC-MS.

Further, the **PIM** formation was supported by the ¹H NMR of the red and yellow solids in DMSO-d⁶ (Fig. S19 and S20, ESI†), which indicates the presence of **BIZM** with its active methylene group and distinct changes of alkene-*H* to imine-*H*. As further support, this imine product, **PIM**, was further reduced with Na[BH₃CN], which generated the expected reduced amine along with many other possible mono-/bis-/cyclic amines.

We could identify some of these products from HPLC/LC-MS analysis, as listed in Fig. S21 (ESI†). Thus, the mechanistic insights of the fluorimetric responses could be elucidated with various experimental observations.

Hence, we report a new class of benzimidazole-based red AIEgen/solid emitters in a facile synthetic strategy and establish an original emissive platform for the aza-Michael addition and subsequent reverse Knoevenagel reactions. Research is ongoing to enhance the fluorescence intensity of this probe by selecting a suitable central core and methylated BIZ units. Among various amine vapors, crucial BAs displayed visually detectable emission variation at different vapor concentrations. Such a strategy develops
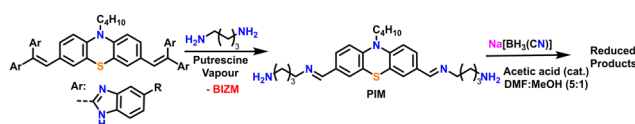

Fig. 7 Reaction of diamines with the probe and reduction of imine (PIM) to support its formation.

new emissive Michael acceptors that enrich historically renowned Michael addition chemistry and provide practical solutions to detect crucial BA vapors for monitoring food spoilage.

Data availability

The data supporting this article have been included as part of the ESI.† This study was carried out using publicly available data that are mentioned in the manuscript.

Conflicts of interest

There are no conflicts to declare.

Notes and references

1 R. S. Keri, A. Hiremathad, S. Budagumpi and B. M. Nagaraja, *Chem. Biol. Drug Des.*, 2015, **86**, 799–845.
2 P. Molina, A. Tarraga and F. Oton, *Org. Biomol. Chem.*, 2012, **10**, 1711–1724.
3 M. Y. Lai, C. H. Chen, W. S. Huang, J. T. Lin, T. H. Ke, L. Y. Chen, M. H. Tsai and C. Wu, *Angew. Chem., Int. Ed.*, 2008, **47**, 581–585.
4 P. Singla, V. Luxami and K. Paul, *RSC Adv.*, 2014, **4**, 12422.
5 E. Horak, P. Kassal and S. I. Murković, *Supramol. Chem.*, 2018, **30**, 838–857.
6 A. Mishra, S. Chatterjee and G. Krishnamoorthy, *J. Photochem. Photobiol., A*, 2013, **260**, 50–58.
7 M. M. Henary, Y. Wu, J. Cody, S. Sumalekshmy, J. Li, S. Mandal and C. J. Fahrni, *J. Org. Chem.*, 2007, **72**, 4784–4797.
8 V. S. Patil, V. S. Padalkar, A. B. Tathe, V. D. Gupta and N. Sekar, *J. Fluoresc.*, 2013, **23**, 1019–1029.
9 J. Luo, Z. Xie, J. W. Y. Lam, L. Cheng, H. Chen, C. Qiu, H. S. Kwok, X. Zhan, Y. Liu, D. Zhu and B. Z. Tang, *Chem. Commun.*, 2001, 1740–1741.
10 B. K. An, S. K. Kwon, S. D. Jung and S. Y. Park, *J. Am. Chem. Soc.*, 2002, **124**, 14410.
11 J. Mei, N. L. C. Leung, R. T. K. Kwok, J. W. Y. Lam and B. Z. Tang, *Chem. Rev.*, 2015, **115**, 11718–11940.
12 W. Yin, W. Li, N. Li, W. Yang, H. An, J. Gao, Y. Bi and N. Zhao, *Adv. Opt. Mater.*, 2020, **8**, 1902027.
13 P. Shen, Z. Zhuang, Z. Zhao and B. Z. Tang, *J. Mater. Chem. C*, 2018, **6**, 11835.
14 Z. Zhao, B. He and B. Z. Tang, *Chem. Sci.*, 2015, **6**, 5347–5365.
15 A. Gogoi, S. Mukherjee, A. Ramesh and G. Das, *Anal. Chem.*, 2015, **87**, 6974–6979.
16 Z. Lu, Y. Liu, S. Lu, Y. Li, X. Liu, Y. Qin and L. Zheng, *RSC Adv.*, 2018, **8**, 19701.
17 R. G. Arnold, R. S. Barrows and R. A. Brooks, *J. Org. Chem.*, 1958, **23**, 565–568.
18 L. Shi, Y. Fu, C. He, D. Zhu, Y. Gao, Y. Wang, Q. He, H. Cao and J. Cheng, *Chem. Commun.*, 2014, **50**, 872.
19 B. Prusti, S. Tripathi, A. Jain and M. Chakravarty, *ACS Appl. Mater. Interfaces*, 2023, **15**, 16492–16504.
20 I. Al-Bulushi, S. Poole, H. C. Deeth and G. A. Dykes, *Crit. Rev. Food Sci.*, 2009, **49**, 369–377.
21 S. L. Taylor, *Crit. Rev. Toxicol.*, 1986, **17**, 91–128.
22 (a) R. Roy, A. Pramanik, T. Dutta, V. K. Sharma and A. L. Koner, *Mater. Chem. Front.*, 2022, **6**, 3489–3503; (b) L. Zeng, X. Xiao, H. Ye, D. Ma and J. Zhou, *Food Chem.*, 2022, **394**, 133489.
23 P. P. Kattimani, R. R. Kamble and G. Y. Meti, *RSC Adv.*, 2015, **5**, 29447–29455.
24 B. Valeur, *Mol. Fluoresc.*, 2009, 477–531.
25 E. Fresch and E. Collini, *Molecules*, 2023, **28**, 3553.
26 F. Würthner, E. Kaiser and C. R. Saha-Möller, *Angew. Chem., Int. Ed.*, 2011, **50**, 3376–3410.
27 X.-Y. Xu, X. Lian, J.-N. Hao, C. Zhang and B. Yan, *Adv. Mater.*, 2017, **29**, 1702298.
28 G. Vinci and M. L. Antonelli, *Food Control*, 2002, **13**, 519–524.
29 G. Zhang, A. S. Loch and P. E. Shaw, *J. Mater. Chem. C*, 2020, **8**, 13723.
30 Y. Cao, M. Yang, Y. Wang, H. Zhou, J. Zheng, X. Zhang, J. Wu, Y. Tian and Z. Wu, *J. Mater. Chem. C*, 2014, **2**, 3686.